Properties and evolution of protoneutron stars within the extended Zimanyi-Moszkowski model

K. Miyazaki

E-mail: miyazakiro@rio.odn.ne.jp

Abstract

We have investigated the properties of protoneutron stars (PNSs) in three different stages during its evolution. Their equations-of-state (EOSs) are derived by the extended Zimanyi-Moszkowski (EZM) model of the relativistic mean-field theory. We have taken into account the isovector-scalar meson and the NSC97f hyperon-hyperon interactions are implemented in terms of appropriate strange-meson coupling constants. The EOSs of the neutrino-trapped PNSs are stiffer than the neutrino-free neutron stars (NSs), while the EOSs of early and late stage of PNSs and of deleptonized hot and cold NSs are nearly the same. As a result, the evolution of NS mass proceeds mostly during the deleptonization. However, the minimum mass is determined in the lepton-rich PNS at the earliest stage of evolution while the maximum mass is determined in the hot deleptonized NS before the final cooling process. The resultant allowed gravitational NS mass between $1.06M_{\odot}$ and $1.604M_{\odot}$ is consistent with the observed masses within $1.35 \pm 0.27M_{\odot}$.

1 Introduction

A neutron star (NS) is born in a stellar remnant after successful supernova explosion. The newly born NS is quite different from the NS observed as a radio pulsar. It is a hot and lepton rich object and so is called a protoneutron star (PNS) [1]. The evolution of PNS is dominated by the deleptonization through neutrino diffusion and the subsequent cooling. The diffused neutrinos are observed by terrestrial detectors and provide unique information on the supernova and the PNS. Nevertheless, the PNS is in quasi-stationary β-equilibrium state during its evolution because the time scale of the weak interaction is much shorter than the time scale of neutrino diffusion. We can therefore investigate the macrophysical evolution of PNS [2-5] in three different stages. An early-type protoneutron star (EPNS) formed during 0.1 to 1 seconds after core bounce is composed of a hot shocked envelope with entropy per baryon $s \sim 5$ and an unshocked core with $s \sim 1$. A late-type protoneutron star (LPNS) formed during 1 to 3 seconds after core bounce is thermally homogenous object with $s \sim 2$. Next, during 10 to 30 seconds after core bounce the PNS is deleptonized and so a hot neutrino-free neutron star (HNS) with $s \sim 1$ is formed. Finally, during the following minutes the HNS cools down to a cold neutron star (CNS).

The most important microphysical ingredient for the macrophysical evolution of PNS is the equation-of-state (EOS) of dense hadronic matter [6]. For calculating the EOS the relativistic mean-field (RMF) theories [7] are more suitable than the nonrelativistic ones. In fact, they are widely used in recent investigations [2,5,8-12]. However, the reliable EOS requires reasonable description of baryon-baryon interactions irrespective of relativistic or nonrelativistic theory. Unfortunately, most of the relativistic EOSs do not take into account the effect of isovector scalar meson, which is crucial for isospin asymmetric hadronic medium. It strongly affects [13] the symmetry energy of nuclear matter and produces the mass splitting between a proton and a neutron in the medium. Moreover, most of the RMF models, as well as the recent nonrelativistic Brueckner-Bethe-Goldstone theory [14], do not consider the hyperon-hyperon (YY) interactions because they are not well known at present. In the RMF theories, the (hidden) strange mesons [15] are necessary so as to treat YY interactions explicitly.

So far, only the work of Ref. [11] has taken into account both the contributions within the RMF theory of PNS. It employed the SU(3)-enlarged nonlinear Walecka model [16] and the Zimanyi-Moszkowski (ZM) model [17]. However, the former model contains too many coupling constants that cannot be well determined from our present knowledge of YY interactions. Moreover, it is decisively important in the investigation of PNS that the employed model is valid at finite temperature. At present, the relatively reliable criterion for the validity is the possibility to reproduce the critical temperature in the liquid-gas phase transition of warm nuclear matter. In this respect, the nonlinear Walecka model [18] cannot reproduce the empirical value [19] of the temperature $T_C = 16.6 \pm 0.86\,\mathrm{MeV}$, while the ZM model [20] can reproduce it fairly well. However, the ZM model predicts the effective mass $m^* = 0.85$ of a nucleon in saturated nuclear matter, which is too large to reproduce the spin-orbit splitting of finite nuclei [21,22]. Moreover, its naïve extension [23-26] to the strange sectors is not confirmed.

Recently, the present author has developed [27] the extended Zimanyi-Moszkowski (EZM) model, which has effective density-dependent meson-baryon coupling constants and reproduces the same saturation properties of nuclear matter as the Dirac-Brueckner-Hartree-Fock theory [28]. Because it is based on the constituent quark model of baryons, its extension to hyperons and strange mesons is uniquely determined. The model has been applied to asymmetric nuclear matter [29], strange hadronic matter [30], neutron star [31] and antikaon condensation [32]. It is also able to predict [33] the critical temperature of nuclear matter. The EZM model was further applied to PNS [34] so as to investigate the possibility of the delayed collapse [8] of a PNS to a low-mass black hole (BH) although we did not take into account the effect of temperature. In the present paper, we extend the investigation of Ref. [34] to EPNS, LPNS and HNS mentioned above. In the next section the EZM model for hot PNS matter will be developed. In section 3, following Ref. [5] we investigate the properties of PNS at each stage in its evolution, and the maximum and minimum masses of NSs. The results of this work are summarized in section 4.

2 The EZM model of PNS

The EZM model for CNS matter taking into account the isovector-scalar meson δ and the (hidden) strange mesons σ^* and ϕ [15] has already been developed in Ref. [31]. In the following we will extend it to finite temperature. The thermodynamic potential per volume $\tilde{\Omega} \equiv \Omega/V$ of PNS matter at temperature T is

$$\begin{aligned}
\tilde{\Omega} &= \frac{1}{2} m_\sigma^2 \langle\sigma\rangle^2 + \frac{1}{2} m_\delta^2 \langle\delta_3\rangle^2 + \frac{1}{2} m_{\sigma^*}^2 \langle\sigma^*\rangle^2 - \frac{1}{2} m_\omega^2 \langle\omega_0\rangle^2 - \frac{1}{2} m_\rho^2 \langle\rho_{03}\rangle^2 - \frac{1}{2} m_\phi^2 \langle\phi_0\rangle^2 \\
&- 2T \sum_{\substack{B=p,n,\Lambda,\Sigma^+, \\ \Sigma^0,\Sigma^-,\Xi^0,\Xi^-}} \int_0^\infty \frac{d^3\mathbf{k}}{(2\pi)^3} \left\{ \ln\left[1+\exp\left(\frac{\nu_B - E^*_{kB}}{T}\right)\right] + \ln\left[1+\exp\left(\frac{-\nu_B - E^*_{kB}}{T}\right)\right] \right\} \\
&- T \sum_{l=e^-,\mu^-,\nu_e,\nu_\mu} \gamma_l \int_0^\infty \frac{d^3\mathbf{k}}{(2\pi)^3} \left\{ \ln\left[1+\exp\left(\frac{\mu_l - e_{kl}}{T}\right)\right] + \ln\left[1+\exp\left(\frac{-\mu_l - e_{kl}}{T}\right)\right] \right\},
\end{aligned} \tag{1}$$

where $M^*_B = m^*_B M_B$ and $E^*_{kB} = (\mathbf{k}^2 + M^{*2}_B)^{1/2}$ are the effective mass and the energy of each baryon in PNS, and μ_l and $e_{kl} = (\mathbf{k}^2 + m_l^2)^{1/2}$ are the chemical potential and the energy of each lepton. In this work we set the Boltzmann constant as a unit. The spin-isospin degeneracy factor for leptons is defined as $\gamma_l = \{2, 2, 1\}$ for $l = \{e, \mu, \nu\}$. The ν_B is given by the chemical potential μ_B and the vector potential V_{0B} of each baryon as

$$\nu_B = \mu_B - V_{0B}. \tag{2}$$

The scalar mean-fields $\langle\sigma\rangle$, $\langle\delta_3\rangle$ and $\langle\sigma^*\rangle$ are determined [31] from the three independent effective masses of p, n and Λ:

$$\bar{\sigma}_N = \frac{\left(1 - m^*_p\right) g^*_{nn\delta} + \left(1 - m^*_n\right) g^*_{pp\delta}}{D_{SN}} g_{NN\sigma}, \tag{3}$$

$$\bar{\delta}_N = \frac{\left(m^*_n - 1\right) g^*_{pp\sigma} - \left(m^*_p - 1\right) g^*_{nn\sigma}}{D_{SN}} g_{NN\delta}, \tag{4}$$

$$\bar{\sigma}^*_\Lambda = \frac{2\left(1 - m^*_\Lambda\right) - \left[2 - \frac{1}{2}\left(1 - m^*_\Lambda\right)\right] \bar{\sigma}_\Lambda}{2 - \frac{1}{2}\left(2 + m^*_\Lambda\right) \bar{\sigma}_\Lambda}, \tag{5}$$

where

$$D_{SN} = g^*_{pp\sigma}\, g^*_{nn\delta} + g^*_{nn\sigma}\, g^*_{pp\delta}, \tag{6}$$

and we have introduced the reduced scalar mean-fields for each baryon,

$$\bar{\sigma}_B \equiv \frac{g_{BB\sigma}}{M_B} \langle\sigma\rangle\,, \tag{7}$$

$$\bar{\delta}_B \equiv \frac{g_{BB\delta}}{M_B} \langle \delta_3 \rangle \,, \tag{8}$$

$$\bar{\sigma}^*_Y \equiv \frac{g_{YY\sigma^*}}{M_Y} \langle \sigma^* \rangle \,. \tag{9}$$

The effective coupling constant $g^*_{pp\sigma}$ *etc.* will be shown later.

The effective masses of Σ and Ξ are given [31] by

$$m^*_{\Sigma^+} = \frac{2 - (3/2)\left(\bar{\sigma}_\Sigma + \bar{\delta}_\Sigma\right) - 2\,\bar{\sigma}^*_\Sigma + \left(\bar{\sigma}_\Sigma + \bar{\delta}_\Sigma\right)\bar{\sigma}^*_\Sigma}{D_{S\Sigma^+}}, \tag{10}$$

$$m^*_{\Sigma^0} = \frac{2 - (3/2)\,\bar{\sigma}_\Sigma - 2\,\bar{\sigma}^*_\Sigma + \bar{\sigma}_\Sigma\,\bar{\sigma}^*_\Sigma}{D_{S\Sigma^0}}, \tag{11}$$

$$m^*_{\Sigma^-} = \frac{2 - (3/2)\left(\bar{\sigma}_\Sigma - \bar{\delta}_\Sigma\right) - 2\,\bar{\sigma}^*_\Sigma + \left(\bar{\sigma}_\Sigma - \bar{\delta}_\Sigma\right)\bar{\sigma}^*_\Sigma}{D_{S\Sigma^-}}, \tag{12}$$

$$m^*_{\Xi^0} = \frac{2 - 2\left(\bar{\sigma}_\Xi + \bar{\delta}_\Xi\right) - (3/2)\,\bar{\sigma}^*_\Xi + \left(\bar{\sigma}_\Xi + \bar{\delta}_\Xi\right)\bar{\sigma}^*_\Xi}{D_{S\Xi^0}}, \tag{13}$$

$$m^*_{\Xi^-} = \frac{2 - 2\left(\bar{\sigma}_\Xi - \bar{\delta}_\Xi\right) - (3/2)\,\bar{\sigma}^*_\Xi + \left(\bar{\sigma}_\Xi - \bar{\delta}_\Xi\right)\bar{\sigma}^*_\Xi}{D_{S\Xi^-}}, \tag{14}$$

where

$$D_{S\Sigma^+} = 2 + \frac{1}{2}\left(1 - \bar{\sigma}^*_\Sigma\right)\left(\bar{\sigma}_\Sigma + \bar{\delta}_\Sigma\right), \tag{15}$$

$$D_{S\Sigma^0} = 2 + \frac{1}{2}\left(1 - \bar{\sigma}^*_\Sigma\right)\bar{\sigma}_\Sigma, \tag{16}$$

$$D_{S\Sigma^-} = 2 + \frac{1}{2}\left(1 - \bar{\sigma}^*_\Sigma\right)\left(\bar{\sigma}_\Sigma - \bar{\delta}_\Sigma\right), \tag{17}$$

$$D_{S\Xi^0} = 2 + \frac{1}{2}\left[1 - \left(\bar{\sigma}_\Xi + \bar{\delta}_\Xi\right)\right]\bar{\sigma}^*_\Xi, \tag{18}$$

$$D_{S\Xi^-} = 2 + \frac{1}{2}\left[1 - \left(\bar{\sigma}_\Xi - \bar{\delta}_\Xi\right)\right]\bar{\sigma}^*_\Xi. \tag{19}$$

The vector mean-fields are determined from the three independent vector potentials of p, n and Λ:

$$\langle \omega_0 \rangle = \frac{g^*_{nn\rho} V_{0p} + g^*_{pp\rho} V_{0n}}{D_{VN}}, \tag{20}$$

$$\langle \rho_{03} \rangle = \frac{g^*_{nn\omega} V_{0p} - g^*_{pp\omega} V_{0n}}{D_{VN}}, \tag{21}$$

$$\langle \phi_0 \rangle = \frac{V_{0\Lambda} - g^*_{\Lambda\Lambda\omega} \langle \omega_0 \rangle}{g^*_{\Lambda\Lambda\phi}}, \tag{22}$$

where

$$D_{VN} = g^*_{pp\omega}\, g^*_{nn\rho} + g^*_{nn\omega}\, g^*_{pp\rho}. \tag{23}$$

The vector potentials of Σ and Ξ are given by

$$V_{0Y} = g^*_{YY\omega}\, \langle \omega_0 \rangle + g^*_{YY\rho}\, \langle \rho_{03} \rangle\, I_{3Y} + g^*_{YY\phi}\, \langle \phi_0 \rangle\,, \tag{24}$$

where $I_{3B} = \{\, 1, -1, 0, 1, 0, -1, 1, -1 \,\}$ for $B = \{\, p, n, \Lambda, \Sigma^+, \Sigma^0, \Sigma^-, \Xi^0, \Xi^- \}$.

The renormalized coupling constants of nucleons in the above equations are given [29] by

$$g^*_{pp\sigma(\omega)} = \left[(1 - \lambda_N) + \lambda_N m^*_p \right] g_{NN\sigma(\omega)}, \tag{25}$$

$$g^*_{nn\sigma(\omega)} = \left[(1 - \lambda_N) + \lambda_N m^*_n \right] g_{NN\sigma(\omega)}, \tag{26}$$

$$g^*_{pp\delta(\rho)} = \left[(1 - \lambda_N) + \lambda_N \left(2m^*_n - m^*_p \right) \right] g_{NN\delta(\rho)}, \tag{27}$$

$$g^*_{nn\delta(\rho)} = \left[(1 - \lambda_N) + \lambda_N \left(2m^*_p - m^*_n \right) \right] g_{NN\delta(\rho)}, \tag{28}$$

where $g_{NN\sigma(\omega,\delta,\rho)}$ is the free coupling constant and $\lambda_N = 1/3$.

The renormalized meson-Λ coupling constants are

$$g^*_{\Lambda\Lambda\sigma(\omega)} = \frac{2 - \bar{\sigma}^*_\Lambda}{D_{S\Lambda}}\, g_{\Lambda\Lambda\sigma(\omega)}. \tag{29}$$

$$g^*_{\Lambda\Lambda\sigma^*(\phi)} = \frac{2 - (1/2)\, \bar{\sigma}_\Lambda}{D_{S\Lambda}}\, g_{\Lambda\Lambda\sigma^*(\phi)}, \tag{30}$$

where

$$D_{S\Lambda} = 2 + \frac{1}{2}\, (1 - \bar{\sigma}^*_\Lambda)\, \bar{\sigma}_\Lambda. \tag{31}$$

The renormalized meson-Σ^0 coupling constants have the same forms as those of Λ:

$$g^*_{\Sigma^0\Sigma^0\sigma(\omega)} = \frac{2 - \bar{\sigma}^*_\Sigma}{D_{S\Sigma^0}}\, g_{\Sigma\Sigma\sigma(\omega)}. \tag{32}$$

$$g^*_{\Sigma^0\Sigma^0\sigma^*(\phi)} = \frac{2 - (1/2)\, \bar{\sigma}_\Sigma}{D_{S\Sigma^0}}\, g_{\Sigma\Sigma\sigma^*(\phi)}. \tag{33}$$

On the other hand, for charged Σs we have

$$g^*_{\Sigma^+\Sigma^+\sigma(\omega,\delta,\rho)} = \frac{2 - \bar{\sigma}^*_\Sigma}{D_{S\Sigma^+}}\, g_{\Sigma\Sigma\sigma(\omega,\delta,\rho)}, \tag{34}$$

$$g^*_{\Sigma^+\Sigma^+\sigma^*(\phi)} = \frac{2 - (1/2)\left(\bar{\sigma}_\Sigma + \bar{\delta}_\Sigma \right)}{D_{S\Sigma^+}}\, g_{\Sigma\Sigma\sigma^*(\phi)}, \tag{35}$$

$$g^*_{\Sigma^-\Sigma^-\sigma(\omega,\delta,\rho)} = \frac{2 - \bar{\sigma}^*_\Sigma}{D_{S\Sigma^-}}\, g_{\Sigma\Sigma\sigma(\omega,\delta,\rho)}, \tag{36}$$

$$g^*_{\Sigma^-\Sigma^-\sigma^*(\phi)} = \frac{2-(1/2)\left(\bar{\sigma}_\Sigma - \bar{\delta}_\Sigma\right)}{D_{S\Sigma^-}}\, g_{\Sigma\Sigma\sigma^*(\phi)}. \tag{37}$$

The renormalized meson-Ξ coupling constants are

$$g^*_{\Xi^0\Xi^0\sigma(\omega,\delta,\rho)} = \frac{2-(1/2)\,\bar{\sigma}^*_\Xi}{D_{S\Xi^0}}\, g_{\Xi\Xi\sigma(\omega,\delta,\rho)}, \tag{38}$$

$$g^*_{\Xi^0\Xi^0\sigma^*(\phi)} = \frac{2-\left(\bar{\sigma}_\Xi + \bar{\delta}_\Xi\right)}{D_{S\Xi^0}}\, g_{\Xi\Xi\sigma^*(\phi)}, \tag{39}$$

$$g^*_{\Xi^-\Xi^-\sigma(\omega,\delta,\rho)} = \frac{2-(1/2)\,\bar{\sigma}^*_\Xi}{D_{S\Xi^-}}\, g_{\Xi\Xi\sigma(\omega,\delta,\rho)}, \tag{40}$$

$$g^*_{\Xi^-\Xi^-\sigma^*(\phi)} = \frac{2-\left(\bar{\sigma}_\Xi - \bar{\delta}_\Xi\right)}{D_{S\Xi^-}}\, g_{\Xi\Xi\sigma^*(\phi)}. \tag{41}$$

All the above quantities are calculated from the effective masses m^*_p, m^*_n and m^*_Λ and the vector potentials V_{0p}, V_{0n} and $V_{0\Lambda}$, which are determined by extremizing the thermodynamic potential $\tilde{\Omega}$ by them:

$$\rho_{bp} + \sum_{Y\neq\Lambda} \frac{g^*_{YY\omega}\, g^*_{nn\rho} + I_{3Y}\, g^*_{YY\rho}\, g^*_{nn\omega} - C_{V\Lambda} g^*_{YY\phi}\, g^*_{nn\rho}}{D_{VN}} \rho_{bY}$$
$$- \frac{g^*_{nn\rho} m^2_\omega \langle\omega_0\rangle + g^*_{nn\omega} m^2_\rho \langle\rho_{03}\rangle - C_{V\Lambda} g^*_{nn\rho} m^2_\phi \langle\phi_0\rangle}{D_{VN}} = 0, \tag{42}$$

$$\rho_{bn} + \sum_{Y\neq\Lambda} \frac{g^*_{YY\omega}\, g^*_{pp\rho} - I_{3Y}\, g^*_{YY\rho}\, g^*_{pp\omega} - C_{V\Lambda} g^*_{YY\phi}\, g^*_{pp\rho}}{D_{VN}} \rho_{bY}$$
$$- \frac{g^*_{pp\rho} m^2_\omega \langle\omega_0\rangle - g^*_{pp\omega} m^2_\rho \langle\rho_{03}\rangle - C_{V\Lambda} g^*_{pp\rho} m^2_\phi \langle\phi_0\rangle}{D_{VN}} = 0, \tag{43}$$

$$\rho_{b\Lambda} + \sum_{Y\neq\Lambda} \frac{g^*_{YY\phi}}{g^*_{\Lambda\Lambda\phi}} \rho_{bY} - \left(\frac{m_\phi}{g^*_{\Lambda\Lambda\phi}}\right)^2 \left(V_{0\Lambda} - g^*_{\Lambda\Lambda\omega} \langle\omega_0\rangle\right) = 0, \tag{44}$$

$$M_p \rho_{sp} + \sum_{Y\neq\Lambda} \frac{\partial m^*_Y}{\partial m^*_p} M_Y \rho_{sY} + \sum_{Y\neq\Lambda} \frac{\partial V_{0Y}}{\partial m^*_p} M_Y \rho_{bY}$$
$$+ m^2_\sigma \langle\sigma\rangle \frac{\partial \langle\sigma\rangle}{\partial m^*_p} + m^2_\delta \langle\delta_3\rangle \frac{\partial \langle\delta_3\rangle}{\partial m^*_p} + m^2_{\sigma^*} \langle\sigma^*\rangle \frac{\partial \langle\sigma^*\rangle}{\partial m^*_p}$$
$$- m^2_\omega \langle\omega_0\rangle \frac{\partial \langle\omega_0\rangle}{\partial m^*_p} - m^2_\rho \langle\rho_{03}\rangle \frac{\partial \langle\rho_{03}\rangle}{\partial m^*_p} - m^2_\phi \langle\phi_0\rangle \frac{\partial \langle\phi_0\rangle}{\partial m^*_p} = 0, \tag{45}$$

$$M_n\rho_{sn}+\sum_{Y\neq\Lambda}\frac{\partial m_Y^*}{\partial m_n^*}M_Y\rho_{sY}+\sum_{Y\neq\Lambda}\frac{\partial V_{0Y}}{\partial m_n^*}M_Y\rho_{bY}$$
$$+\,m_\sigma^2\left\langle\sigma\right\rangle\frac{\partial\left\langle\sigma\right\rangle}{\partial m_n^*}+m_\delta^2\left\langle\delta_3\right\rangle\frac{\partial\left\langle\delta_3\right\rangle}{\partial m_n^*}+m_{\sigma^*}^2\left\langle\sigma^*\right\rangle\frac{\partial\left\langle\sigma^*\right\rangle}{\partial m_n^*}$$
$$-\,m_\omega^2\left\langle\omega_0\right\rangle\frac{\partial\left\langle\omega_0\right\rangle}{\partial m_n^*}-m_\rho^2\left\langle\rho_{03}\right\rangle\frac{\partial\left\langle\rho_{03}\right\rangle}{\partial m_n^*}-m_\phi^2\left\langle\phi_0\right\rangle\frac{\partial\left\langle\phi_0\right\rangle}{\partial m_n^*}=0, \tag{46}$$

$$M_\Lambda\rho_{s\Lambda}+\sum_{Y\neq\Lambda}\frac{\partial m_Y^*}{\partial m_\Lambda^*}M_Y\rho_{sY}+\sum_{Y\neq\Lambda}\frac{\partial V_{0Y}}{\partial m_\Lambda^*}\rho_{bY}+m_{\sigma^*}^2\left\langle\sigma^*\right\rangle\frac{\partial\left\langle\sigma^*\right\rangle}{\partial m_\Lambda^*}-m_\phi^2\left\langle\phi_0\right\rangle\frac{\partial\left\langle\phi_0\right\rangle}{\partial m_\Lambda^*}=0, \tag{47}$$

where $C_{V\Lambda}=g_{\Lambda\Lambda\omega}^*/g_{\Lambda\Lambda\phi}^*$. The calculations of the derivatives in Eqs. (42)-(47) are tedious but straightforward tasks and so their expressions are not shown explicitly.

The baryon and scalar densities of each baryon in Eqs. (42)-(47) are defined by

$$\rho_{bB}=2\int_0^\infty\frac{d^3\mathbf{k}}{(2\pi)^3}\left[n_{kB}\left(T\right)-\bar{n}_{kB}\left(T\right)\right], \tag{48}$$

$$\rho_{sB}=2\int_0^\infty\frac{d^3\mathbf{k}}{(2\pi)^3}\frac{M_B^*}{E_{kB}^*}\left[n_{kB}\left(T\right)+\bar{n}_{kB}\left(T\right)\right], \tag{49}$$

where the Fermi-Dirac distribution functions of each baryon and antibaryon are

$$n_{kB}\left(T\right)=\left[1+\exp\left(\frac{E_{kB}^*-\nu_B}{T}\right)\right]^{-1}, \tag{50}$$

$$\bar{n}_{kB}\left(T\right)=\left[1+\exp\left(\frac{E_{kB}^*+\nu_B}{T}\right)\right]^{-1}. \tag{51}$$

Similarly, the density of each lepton is defined by

$$\rho_l=\gamma_l\int_0^\infty\frac{d^3\mathbf{k}}{(2\pi)^3}\left[n_{kl}\left(T\right)-\bar{n}_{kl}\left(T\right)\right], \tag{52}$$

where the Fermi-Dirac distribution functions of each lepton and antilepton are

$$n_{kl}\left(T\right)=\left[1+\exp\left(\frac{e_{kl}-\mu_l}{T}\right)\right]^{-1}, \tag{53}$$

$$\bar{n}_{kl}\left(T\right)=\left[1+\exp\left(\frac{e_{kl}+\mu_l}{T}\right)\right]^{-1}. \tag{54}$$

Finally, the energy density of PNS matter is given by

$$\begin{aligned}\mathcal{E} &= \frac{1}{2}m_\sigma^2\langle\sigma\rangle^2+\frac{1}{2}m_\delta^2\langle\delta_3\rangle^2+\frac{1}{2}m_{\sigma^*}^2\langle\sigma^*\rangle^2-\frac{1}{2}m_\omega^2\langle\omega_0\rangle^2-\frac{1}{2}m_\rho^2\langle\rho_{03}\rangle^2-\frac{1}{2}m_\phi^2\langle\phi_0\rangle^2 \\ &+2\sum_{\substack{B=p,n,\Lambda,\Sigma^+,\\ \Sigma^0,\Sigma^-,\Xi^0,\Xi^-}}\left\{\left(\int_0^\infty\frac{d^3\mathbf{k}}{(2\pi)^3}E_{kB}^*\left[n_{kB}(T)+\bar{n}_{kB}(T)\right]\right)+V_{0B}\rho_{bB}\right\} \\ &+\sum_{l=e^-,\mu^-,\nu_e,\nu_\mu}\gamma_l\int_0^\infty\frac{d^3\mathbf{k}}{(2\pi)^3}e_{kl}\left[n_{kl}(T)+\bar{n}_{kl}(T)\right], \end{aligned} \tag{55}$$

and the pressure is

$$P=-\tilde{\Omega}. \tag{56}$$

3 Numerical analyses

For calculating dense baryonic matter we have to specify the meson-baryon coupling constants. The $NN\sigma$ and $NN\omega$ coupling constants were determined [27] so as to reproduce the nuclear matter saturation properties. The $NN\delta$ and $NN\rho$ coupling constants are the same as the Bonn A potential in Ref. [28]. As a result, the symmetry-energy of nuclear matter is however lower than its empirical value. On the other hand, most of the RMF calculations do not take into account δ meson but assume stronger $NN\rho$ coupling constant than the Bonn model so as to reproduce the empirical symmetry-energy. If the δ meson is introduced, their $NN\rho$ coupling becomes much stronger [13]. Such an unphysical strong coupling is usually excused by mentioning that the meson-baryon coupling constants in the models are the effective ones. Fortunately or not, the similar cheating is not applicable to the EZM model in which the effective renormalized coupling constants are determined self-consistently in the medium. We therefore have to designate the coupling constant obtained from NN scattering data, not the effective one.

Next, the hyperon coupling constants are considered. The $YY\omega$, $YY\delta$ and $YY\rho$ coupling constants are fixed by the SU(6) relations:

$$\frac{1}{3}g_{NN\omega}=\frac{1}{2}g_{\Lambda\Lambda\omega}=\frac{1}{2}g_{\Sigma\Sigma\omega}=g_{\Xi\Xi\omega}, \tag{57}$$

$$g_{NN\delta}=\frac{1}{2}g_{\Sigma\Sigma\delta}=g_{\Xi\Xi\delta}\quad\text{and}\quad g_{\Lambda\Lambda\delta}=0, \tag{58}$$

$$g_{NN\rho}=\frac{1}{2}g_{\Sigma\Sigma\rho}=g_{\Xi\Xi\rho}\quad\text{and}\quad g_{\Lambda\Lambda\rho}=0. \tag{59}$$

On the other hand, the $YY\sigma$ coupling constants are chosen [16] so as to give the reasonable hyperons potentials in saturated nuclear matter at $\rho_{nm}=0.16\,\mathrm{fm}^{-3}$:

$$U_\Lambda^{(N)}(\rho_{nm})=-28\,\mathrm{MeV},\quad U_\Sigma^{(N)}(\rho_{nm})=30\,\mathrm{MeV}\quad\text{and}\quad U_\Xi^{(N)}(\rho_{nm})=-18\,\mathrm{MeV}. \tag{60}$$

We have obtained

$$\frac{g_{\Lambda\Lambda\sigma}}{g_{NN\sigma}} = 0.604, \quad \frac{g_{\Sigma\Sigma\sigma}}{g_{NN\sigma}} = 0.461 \quad \text{and} \quad \frac{g_{\Xi\Xi\sigma}}{g_{NN\sigma}} = 0.309. \tag{61}$$

Next, the coupling constants of the strange mesons are considered. Although there remain uncertainties [35] in determining them, we here follow the prescription of Ref. [36]. The $YY\phi$ coupling constants are fixed by the SU(6) relations:

$$2\, g_{\Lambda\Lambda\phi} = 2\, g_{\Sigma\Sigma\phi} = g_{\Xi\Xi\phi} = -\frac{2\sqrt{2}}{3} g_{NN\omega}. \tag{62}$$

Then $\Lambda\Lambda\sigma^*$ and $\Xi\Xi\sigma^*$ coupling constants are determined so as to reproduce the binding energy curves of pure Λ and Ξ matter in the Brueckner-Hartree-Fock calculation [37] using the Nijmegen soft-core potential model NSC97f [38,39]. This prescription is reasonable because the Faddeev calculation [40] using the Nijmegen potential can reproduce the recent data of ${}^{\;\;6}_{\Lambda\Lambda}$He [41]. On the other hand, if the $\Sigma\Sigma\sigma^*$ coupling constant is determined in the same way as Λ and Ξ, it becomes quite strong to bring about an unlikely first-order phase transition [30,36,42] from $N + \Lambda + \Xi$ matter to the strange hadronic matter with dominant abundance of Σ. Therefore, in the present work the same $\Sigma\Sigma\sigma^*$ coupling constant as $\Lambda\Lambda\sigma^*$ is assumed according to the SU(6) symmetry. Consequently, we have

$$\frac{g_{\Lambda\Lambda\sigma^*}}{g_{NN\sigma}} = \frac{g_{\Sigma\Sigma\sigma^*}}{g_{NN\sigma}} = 0.52 \quad \text{and} \quad \frac{g_{\Xi\Xi\sigma^*}}{g_{NN\sigma}} = 1.28. \tag{63}$$

As mentioned in Introduction, we investigate PNSs at three different stages in its macrophysical evolution. The configuration of each stage is summarized in Table 1. Although there remain uncertainties [3-5] in specifying the configurations, it is expected that the essential features of the results do not depend on their choices. Because the time scale of the weak interaction is much shorter than the time scale of the evolution, the PNS at each stage is in β-equilibrium:

$$\mu_i = b_i \mu_n - q_i \left(\mu_{e^-} - \mu_{\nu_e}\right), \tag{64}$$

$$\mu_{\mu^-} - \mu_{\nu_\mu} = \mu_{e^-} - \mu_{\nu_e}, \tag{65}$$

where b_i and q_i are the baryon number and the charge of each particle. Therefore, the four chemical potentials of baryon, charge, electro-neutrino and mu-neutrino are independent. They are constrained by the fixed total baryon density (or the baryon number conservation)

$$\rho_T = \sum_{\substack{B=p,n,\Lambda,\Sigma^+,\\ \Sigma^0,\Sigma^-,\Xi^0,\Xi^-}} \rho_{bB}, \tag{66}$$

the charge neutral condition

$$\sum_{i=B,l} q_i \rho_i = 0, \tag{67}$$

and the lepton number conservations [1]

$$Y_{Le} = \frac{\rho_{e^-} + \rho_{\nu_e}}{\rho_T} = 0.4, \tag{68}$$

$$Y_{L\mu} = \frac{\rho_{\mu^-} + \rho_{\nu_\mu}}{\rho_T} = 0. \tag{69}$$

The property of PNS matter under the isentropic condition

$$s = \frac{\mathcal{E} + P - \sum_{i=B,l} \mu_i \rho_i}{T\,\rho_T}, \tag{70}$$

is then determined by solving Eqs. (42)-(47) and (66)-(70) simultaneously in terms of 11-dimensional Newton-Raphson method, so that the effective masses m_p^*, m_n^* and m_Λ^*, the vector potentials V_{0p}, V_{0n} and $V_{0\Lambda}$, the chemical potentials μ_n, μ_{e^-}, μ_{ν_e} and μ_{ν_μ} and the temperature T are determined selfconsistently. For the neutrino-free NS matter, the neutrino chemical potentials disappear and so we solve 9-dimensional nonlinear equations other than Eqs. (68) and (69).

Figures 1-4 show the particle fractions in the cores of PNSs and NSs at each stage of evolution. It is first seen that the hyperons appear at lower densities in EPNS, LPNS and HNS than CNS because of the Fermi-Dirac distribution functions. The similar results are seen in Refs. [2] and [14]. To the contrary, Refs. [10] and [12] predicted that the appearances of hyperons hardly depend on the temperature or entropy. Although the reason is not obvious, their results seem to be questionable.

In Figs. 1 and 2, the neutrino fractions initially decrease as ρ_T increases, but turn to increase above $\rho_T = 0.43\,\mathrm{fm}^{-3}$ and $\rho_T = 0.36\,\mathrm{fm}^{-3}$ after Λ is abundant. Appearances of Ξ^- and then Ξ^0 increase the neutrino fractions further. This can be readily understood from the chemical equilibrium condition $\mu_p = \mu_n - \mu_{e^-} + \mu_{\nu_e}$, because the abundance of hyperons decrease neutron fraction owing to the baryon number conservation (66) while the sum of proton and electron fractions is nearly constant in the whole range of density. In the comparison of Fig. 1 with Fig. 2, at higher entropy the Σ hyperons also appear but their fractions are much lower than Λ and Ξ because of the repulsive potential in Eq. (60). To the contrary, in Ref. [14] the abundance of Ξ^- are replaced by Σ^-. This however suggests that the baryon-baryon interactions employed in Ref. [14] are not physically reasonable because the repulsive potential of Σ^- in nuclear matter has been confirmed in the recent theoretical analyses [43] of (π^-, K^+) inclusive reaction.

In the comparison of Fig. 1 with Fig. 3 we can see the effect of trapped neutrinos in NS matter. Due to the chemical equilibrium condition $\mu_{\Sigma^-} = \mu_n + \mu_{e^-} - \mu_{\nu_e}$ the

appearance of Σ^- in HNS is repressed in EPNS. Because of the chemical equilibrium condition $\mu_p = \mu_n - \mu_{e^-} + \mu_{\nu_e}$ the proton is abundant below $\rho_T = 0.4\,\mathrm{fm}^{-3}$ in PNS matter. As a result, the neutron in EPNS is scarcer than in HNS because of the baryon number conservation (66) and then the appearance of Λ is delayed due to the chemical equilibrium condition $\mu_\Lambda = \mu_n$. To the contrary, the appearance of Ξ^0 is not largely delayed because the proton in HNS matter is already abundant above $\rho_T = 0.5\,\mathrm{fm}^{-3}$. The appearance of Ξ^- in EPNS is also delayed by the abundance of neutrinos because of the chemical equilibrium condition $\mu_{\Xi^-} = \mu_n + \mu_{e^-} - \mu_{\nu_e}$. Moreover, at high density the abundance of electron in EPNS due to the lepton number conservation (68) suppresses Ξ^- as compared with HNS because of the charge neutral condition (67).

Figure 5 shows the temperature profiles of EPNS, LPNS and HNS as functions of the total baryon density. The sharp peak in EPNS below $\rho_T = 0.1\,\mathrm{fm}^{-3}$ is due to the hot shocked envelope in Table 1. In EPNS and HNS the temperatures turn to decrease above $\rho_T = 0.48\,\mathrm{fm}^{-3}$ and $\rho_T = 0.33\,\mathrm{fm}^{-3}$, respectively. They are just above the densities at which Ξ^- appear in Figs. 1 and 3. In the cores of stars with lower entropy $s = 1$, the temperature

$$T = \frac{\mathcal{E} + P}{s\,\rho_T} - \left(\mu_n + Y_{L_e}\mu_{e^-}\right), \tag{71}$$

is determined by the competition of energy and pressure with chemical potentials. The appearance of Ξ^- implies the enough increase of μ_n for the competition. To the contrary, in the core of LPNS with higher entropy $s = 2$ the depletion of temperature disappears because the thermal effect is dominant.

Figure 6 shows the pressures of stars in each stage of evolution as functions of the total baryon density. Because the lepton-rich stars have richer proton than neutrino-free stars due to the charge neutral condition, the hyperons in PNSs are less abundant than NSs. This and the rich leptons lead to the stiffer EOSs of the neutrino-trapped PNSs than the neutrino-free NSs above $\rho_T = 0.4\,\mathrm{fm}^{-3}$. It is also seen in the comparisons of blue curves with red ones that the difference of entropy by $s \sim 1$ has little effects on the pressures except at high densities. This is because the higher thermal pressure in LPNS and HNS is cancelled in part by the softening of EOS due to the earlier appearances of hyperons than in EPNS and CNS.

In Figs. 7 and 8 the gravitational masses of stars in each stage of evolution are calculated as functions of the central energy density and the radius by integrating the Tolman-Oppenheimer-Volkov equation [44]. The nuclear EOSs from the EZM model are extended to the hot subnuclear layers of stars in Table 1, while for the cold outer crust in the region $\rho_T \leq 6 \times 10^{-4}\,\mathrm{fm}^{-3}$ we have employed the EOSs of Feynman-Metropolis-Teller, Baym-Pethick-Sutherland and Negele-Vautherin from Ref. [45]. The EOS of the transition region between the cold outer crust and the hot inner layer in LPNS or HNS is obtained by interpolating their EOSs. Because the EOSs of HNS and CNS are almost

the same as seen in Fig. 6, the differences between the red and the blue dashed curves are little. The differences between EPNS and LPNS are due to the hot shocked envelope in EPNS. It is seen that the maximum masses of neutrino-trapped stars are larger than neutrino-free stars. This suggests [8] the possible delayed collapse of a PNS to a low-mass BH. On the other hand, the minimum mass of EPNS is larger than $M_\odot$. This suggests [4] that the minimum gravitational mass of CNS is determined at the earliest stage of PNS.

In order to investigate the maximum and minimum masses of CNS in more detail, Fig. 9 shows the gravitational-baryonic mass correlation of stars in each stage of evolution because the baryonic mass is conserved during the evolution. The differences between the red and the blue curves are little because the corresponding EOSs in Fig. 6 are almost the same. According to Ref. [8], the PNS with baryonic mass being larger than the maximum mass $M_B = 1.806 M_\odot$ of CNS can be stabilized by trapped-neutrinos but might collapse to a low-mass BH after the deleptonization. We however find that the maximum baryonic mass $M_B = 1.792 M_\odot$ of HNS is slightly lighter than that of CNS. This is also seen in Ref. [5] although the authors did not refer to the fact explicitly. If the evolution of star through the cooling after the deleptonization is proper, the maximum mass of CNS is determined from the maximum mass of HNS. The obtained maximum gravitational mass $M_G = 1.604 M_\odot$ is slightly lower than the maximum value $M_G = 1.615 M_\odot$ of the blue dashed curve in Fig. 7. On the other hand, we can see that the minimum baryonic mass $M_B = 1.138 M_\odot$ of EPNS leads to the minimum gravitational mass $M_G = 1.060 M_\odot$ of CNS. The resultant allowed gravitational NS mass between $1.06 M_\odot$ and $1.60 M_\odot$ is consistent with the observed NS masses within $1.35 \pm 0.27 M_\odot$ [46].

In Tables 2 and 3 we summarize the evolutions of stars with the maximum baryonic mass of HNS and the minimum mass of EPNS. Moreover, Table 4 shows the evolution of stars with the baryonic mass corresponding to the famous canonical value $M_G = 1.441 M_\odot$ [47] of CNS obtained from the relativistic binary pulsar B1913+16. Figures 10 and 11 also show graphically the evolutions of radius and central baryon density. The differences between the properties of HNS and CNS are small except for the central baryon density in the star with the maximum baryonic mass. This is because both the EOSs of HNS and CNS are almost the same as seen in Fig. 6. In the evolution of EPNS to LPNS and then to HNS the stars shrink largely. As the mass is lower, the shrinkage is more striking. This is essentially the thermal effect in the subnuclear layers of stars. The largest radius of EPNS is due to the hot shocked envelope. The larger radius of LPNS than HNS is due to its higher entropy. The central baryon density becomes diluter during the first stage of evolution from EPNS to LPNS, while it becomes denser during the next deleptonization from LPNS to HNS. For the star with the maximum mass the rise of the density is striking. During the final cooling from HNS to CNS, the density becomes diluter or denser in the stars with mass below or above $M_B = 1.53 M_\odot$.

As in Ref. [4] we have found that the minimum gravitational mass of CNS is determined at the earliest stage of PNS. On the other hand, Ref. [48] examined the most likely

masses of NSs based on the simulation of Type-II supernovae and obtained a lower limit of the NS mass $M_G = 1.18M_\odot$. The value is higher than $M_G = 1.06M_\odot$ in Table 3. However, our result depends on the configurations assumed for EPNS, in which there remain some ambiguities [3-5]. Then, we calculate under the other two configurations than Table 3. Assuming that the core of EPNS lies above $\rho_T = 0.15\,\mathrm{fm}^{-3}$ instead of $\rho_T = 0.10\,\mathrm{fm}^{-3}$ we have the minimum baryonic mass $M_B = 1.338M_\odot$ of EPNS. Assuming that the entropy of the hot shocked envelope is $s = 5.5$ instead of $s = 5.0$ we have $M_B = 1.283M_\odot$. The evolutions of the stars with these baryonic masses are summarized in Tables 5 and 6. The resultant minimum gravitational masses of CNS are $M_G = 1.23M_\odot$ and $M_G = 1.18M_\odot$, which agrees with the result of Ref. [48].

4 Summary

We have investigated the properties of PNSs at different stages during its evolution. Their EOSs, the most important microphysical ingredients, have been derived by the new nonlinear RMF model, the EZM model, which reproduces the effective density-dependent meson-baryon coupling constants to be necessary for dense hadronic matter. We have also taken into account the isovector-scalar meson and the (hidden) strange mesons that are indispensable to reasonable description of baryon-baryon interactions. The isovector meson coupling constants have been taken from Bonn A potential. The NSC97f hyperon-hyperon interactions have been implemented in terms of the appropriate strange-meson coupling constants.

The EOSs of the neutrino-free NSs becomes softer than those of the neutrino-trapped PNSs above $\rho_T = 0.4\,\mathrm{fm}^{-3}$, while they do not depend on the difference of entropy per baryon. The temperature in the core with $s = 1$ turns to decrease after Ξ^- is abundant due to the competition of the thermal energy and pressure with the baryonic chemical potential. The evolution of the gravitational mass proceeds mostly during the deleptonization process from LPNS to HNS. To the contrary, the radius remarkably shrinks during the earliest evolution from EPNS to LPNS, but almost converges after the deleptonization. On the other hand, the central baryon density oscillates during the evolution especially in the star of maximum mass. We have found that the maximum baryonic mass $M_B = 1.792M_\odot$ of HNS is lighter than that of CNS. Therefore, if the cooling after the deleptonization is proper, the maximum gravitational mass $M_G = 1.604M_\odot$ of CNS is determined in HNS. On the other hand, due to the hot shocked envelope the EPNS has a minimum baryonic mass larger than $M_\odot$, which determines the minimum gravitational mass $M_G = 1.060M_\odot$ of CNS. The resultant allowed NS mass between $1.06M_\odot$ and $1.60M_\odot$ is consistent with the observed masses within $M_G = 1.35 \pm 0.27M_\odot$. Moreover, we have investigated the uncertainties of the minimum mass due to our assumptions of the configuration in EPNS. If the entropy per baryon $s = 5.5$ is assumed for the shocked envelope, the minimum mass $M_G = 1.18M_\odot$ is obtained. It agrees with the value derived

from the simulation of Type-II supernovae.

References

[1] M. Prakash, I. Bombaci, M. Prakash, P.J. Ellis, R. Knorren and J.M. Lattimer, Phys. Rep. **280** (1997) 1 [arXiv:nucl-th/9603042].

[2] J.A. Pons, S. Reddy, M. Prakash, J.M. Lattimer and J.A. Miralles, Astrophys. J. **513** (1999) 780.

[3] J-O. Goussard, P. Haensel and J.L. Zdunik, Astron. Astrophys. **330** (1998) 1005.

[4] K. Strobel, Ch. Schaab and M.K. Weigel, Astron. Astrophys. **350** (1999) 497.

[5] K. Strobel and M.K. Weigel, Astron. Astrophys. **367** (2001) 582.

[6] J.M. Lattimer and M. Prakash, Astrophys. J. **550** (2001) 426.

[7] B.D. Serot and J.D. Walecka, *Advances in Nuclear Physics*, Vol. **16** (Plenum, New York, 1986).

[8] I. Bombaci, Astron. Astrophys. **305** (1996) 871.

[9] J.A. Pons, S. Reddy, P.J. Ellis, M. Prakash, and J.M. Lattimer, Phys. Rev. **C62** (2000) 035803 [arXiv:nucl-th/0003008].

[10] G.F. Marranghello, C.A.Z. Vasconcellos, M. Dillig and J.A. de F. Pacheco, Int. J. Mod. Phys. **E11** (2002) 83 [arXiv:astro-ph/0107476].

[11] D.P. Menezes and C. Providência, Phys. Rev. **C69** (2004) 045801 [arXiv:nucl-th/0312050].

[12] I. Bednarek, M. Keska and R. Mańka, arXiv:nucl-th/0403060.

[13] S. Kubis and M. Kutschera, Phys. Lett. **B399** (1997) 191 [arXiv:astro-ph/9703049].

[14] O.E. Nicotra, M. Baldo, G.F. Burgio and H.-J. Schultz, arXiv:nucl-th/0506066.

[15] J. Schaffner, C.B. Dover, A. Gal, C. Greiner and H. Stőker, Phys. Rev. Lett. **71** (1993) 1328.

[16] N.K. Glendenning and S.A. Moszkowski, Phys. Rev. Lett. **67** (1991) 2414.

[17] J. Zimanyi and S.A. Moszkowski, Phys. Rev. **C42** (1990) 1416.

[18] H. Müller and B.D. Serot, Phys. Rev. **C52** (1995) 2072 [arXiv:nucl-th/9505013].

[19] J.B. Natowitz *et al.*, Phys. Rev. Lett. **89** (2002) 212701 [arXiv:nucl-ex/0204015].

[20] Z.X. Qian, H.Q. Song and R.K. Su, Phys. Rev. **C48** (1993) 154.

[21] W. Koepf, M.M. Sharma and P. Ring, Nucl. Phys. **A533** (1991) 95.

[22] M.M. Sharma, M.A. Nagarajan and P. Ring, Ann. of Phys. **231** (1994) 110.

[23] N.K. Glendenning, F. Weber and S.A. Moszkowski, Phys. Rev. **C45** (1992) 844.

[24] A.R. Taurines, C.A.Z. Vasconcellos, M. Malheiro and M. Chiapparini, Phys. Rev. **C63** (2001) 065801 [arXiv:nucl-th/0010084].

[25] Z.X. Ma, Z.G. Dai and T. Lu, Astron. Astrophys. **366** (2001) 532.

[26] I. Bednarek, M. Keska and R. Mańka, Phys. Rev. **C68** (2003) 035805 [arXiv:nucl-th/0212065].

[27] K. Miyazaki, Mathematical Physics Preprint Archive (mp_arc) 05-178.

[28] R. Brockmann and R. Machleidt, Phys. Rev. **C42** (1990) 1965.

[29] K. Miyazaki, Mathematical Physics Preprint Archive (mp_arc) 05-190.

[30] K. Miyazaki, Mathematical Physics Preprint Archive (mp_arc) 05-216.

[31] K. Miyazaki, Mathematical Physics Preprint Archive (mp_arc) 05-224.

[32] K. Miyazaki, Mathematical Physics Preprint Archive (mp_arc) 05-233.

[33] K. Miyazaki, Mathematical Physics Preprint Archive (mp_arc) 05-261.

[34] K. Miyazaki, Mathematical Physics Preprint Archive (mp_arc) 05-243.

[35] I. Bednarek and R. Mańka, J. Phys. **G31** (2005) 1009 [arXiv:hep-ph/0506059].

[36] J. Schaffner-Bielich and A. Gal, Phys. Rev. **C62** (2000) 034311 [arXiv:nucl-th/0005060].

[37] V.G.J. Stoks and T.-S.H. Lee, Phys. Rev. **C60** (1999) 024006 [arXiv:nucl-th/9901030].

[38] Th.A. Rijken, V.G.J. Stoks and Y. Yamamoto, Phys. Rev. **C59** (1999) 21 [arXiv:nucl-th/9807082].

[39] V.G.J. Stoks and Th.A. Rijken, Phys. Rev. **C59** (1999) 3009 [arXiv:nucl-th/9901028].

[40] I.N. Filikhin and A. Gal, Phys. Rev. **C65** (2002) 041001(R); Nucl. Phys. **A707** (2002) 491 [arXiv:nucl-th/0203036]; I.N. Filikhin, A. Gal and V.M. Suslov, Phys. Rev. **C68** (2003) 024002 [arXiv:nucl-th/0303028]; Nucl. Phys. **A743** (2004) 194 [arXiv:nucl-th/0406049];

[41] H. Takahashi *et al.*, Phys. Rev. Lett. **87** (2001) 212502.

[42] I. Zakout, H.R. Jaqaman, H. Stöker and W. Greiner, J. Phys. **G27** (2001) 1939 [arXiv:nucl-th/005005].

[43] M. Kohno, Y. Fujiwara, Y. Watanabe, K. Ogata and M. Kawai, arXiv:nucl-th/0410073.

[44] W.D. Arnett and R.L. Bowers, Astrophys. J. Suppl. **33** (1977) 415.

[45] V. Canuto, Ann. Rev. Astr. Ap. **12** (1974) 167; **13** (1975) 335.

[46] S.E. Thorsett, A. Arzoumanian, M.M. McKinnon and J.H. Taylor, Astropys. J. **405** (1993) L29.

[47] J.M. Weisberg and J.H. Taylor, Proceedings of "Radio Pulsars," Chania, Crete, August, 2002, ASP. Conf. Series, 2003, M. Bailes, D. J. Nice, S.E. Thorsett, eds. [arXiv:astro-ph/0211217].

[48] F.X. Timmes, S.E. Woosley and T.A. Weaver, Astrophys. J. **457** (1996) 834.

Table 1: The configurations at each stage in the evolution of PNS. The entropy per baryon s and the lepton fraction Y_{L_e} are specified for each layer in the stars.

	Layer	s	Y_{L_e}
EPNS	$\rho_T \leq 6 \times 10^{-4}\,\mathrm{fm}^{-3}$	0	0.0
	$6 \times 10^{-4}\,\mathrm{fm}^{-3} < \rho_T < 0.02\,\mathrm{fm}^{-3}$	5	0.4
	$\rho_T \geq 0.1\,\mathrm{fm}^{-3}$	1	0.4
LPNS	$\rho_T \leq 6 \times 10^{-4}\,\mathrm{fm}^{-3}$	0	0.0
	$\rho_T \geq 0.06\,\mathrm{fm}^{-3}$	2	0.4
HNS	$\rho_T \leq 6 \times 10^{-4}\,\mathrm{fm}^{-3}$	0	0.0
	$\rho_T \geq 0.06\,\mathrm{fm}^{-3}$	1	0.0

Table 2: The evolution of gravitational mass M_G, radius R, central baryon density ρ_c and central temperature T_c of the stars with the maximum baryonic mass $M_B = 1.792 M_\odot$ of HNS.

	$M_G\,(M_\odot)$	R(km)	$\rho_c(\mathrm{fm}^{-3})$	T_c(MeV)
EPNS	1.675	18.80	0.460	20.0
LPNS	1.698	15.30	0.430	37.9
HNS	1.616	13.15	0.702	20.9
CNS	1.604	13.20	0.572	0.0

Table 3: The same as Table 2 but for the stars with the mimimum baryonic mass $M_B = 1.138 M_\odot$ of EPNS.

	$M_G\,(M_\odot)$	R(km)	$\rho_c(\mathrm{fm}^{-3})$	T_c(MeV)
EPNS	1.125	42.31	0.253	14.3
LPNS	1.121	17.88	0.247	29.2
HNS	1.067	13.93	0.283	19.3
CNS	1.060	13.37	0.297	0.0

Table 4: The same as Table 2 but for the stars with the baryonic mass corresponding to the canonical gravitational mass $M_G = 1.441 M_\odot$ of CNS.

	$M_G\,(M_\odot)$	R(km)	$\rho_c(\mathrm{fm}^{-3})$	T_c(MeV)
EPNS	1.508	21.05	0.393	19.3
LPNS	1.526	16.01	0.356	35.8
HNS	1.451	13.75	0.385	19.4
CNS	1.441	13.37	0.377	0.0

Table 5: The same as Table 3 except that the minimum baryon density of unshocked core in EPNS is $\rho_T = 0.15\,\mathrm{fm}^{-3}$.

	$M_G\,(M_\odot)$	R(km)	$\rho_c(\mathrm{fm}^{-3})$	T_c(MeV)
EPNS	1.314	39.64	0.277	15.3
LPNS	1.304	16.95	0.291	32.3
HNS	1.240	13.88	0.320	20.0
CNS	1.231	13.39	0.330	0.0

Table 6: The same as Table 3 except that the entropy of hot shocked envelope in EPNS is $s = 5.5$.

	$M_G\,(M_\odot)$	R(km)	$\rho_c(\mathrm{fm}^{-3})$	T_c(MeV)
EPNS	1.260	42.95	0.278	15.4
LPNS	1.254	17.18	0.278	31.5
HNS	1.192	13.89	0.309	19.9
CNS	1.184	13.39	0.321	0.0

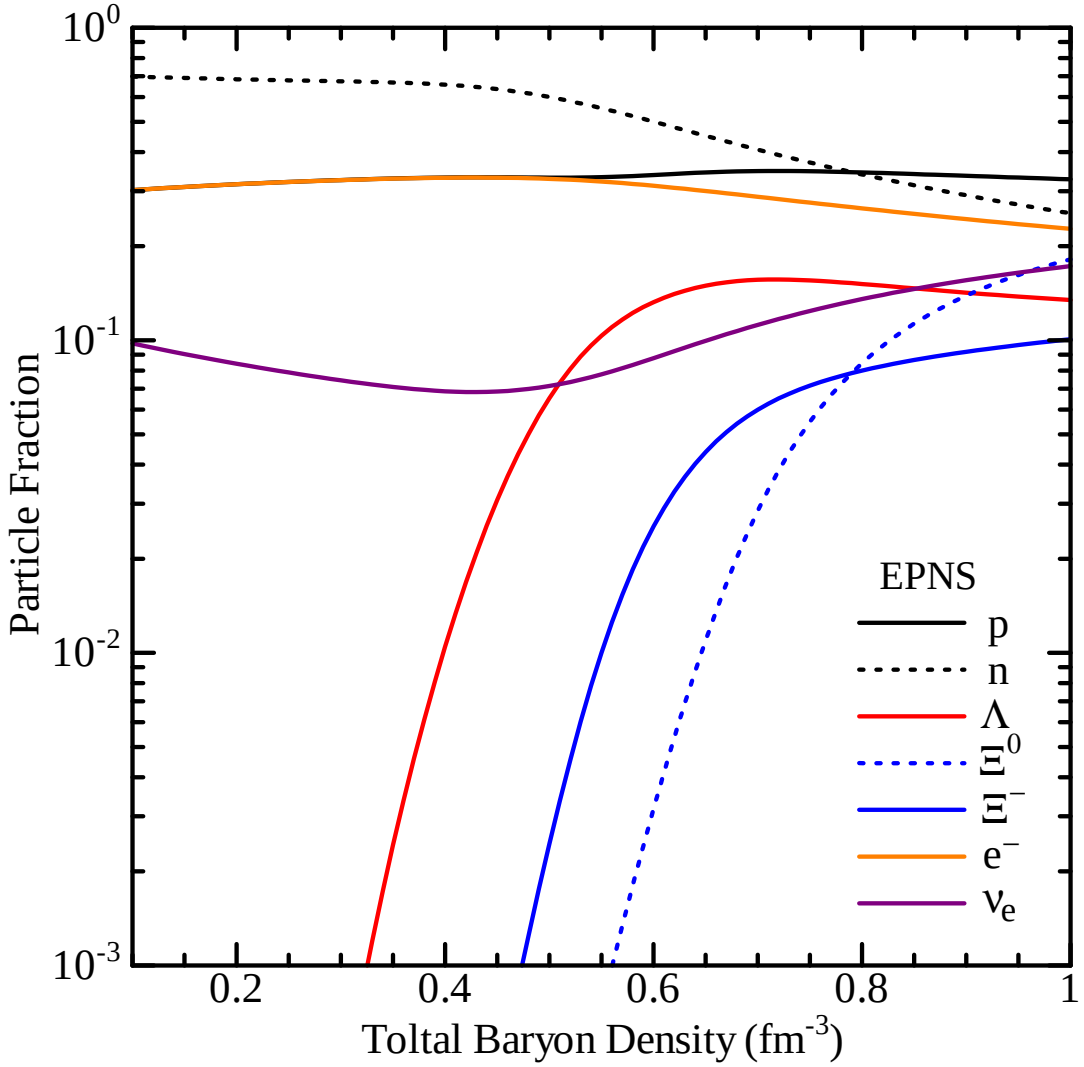

Figure 1: The particle fractions in the core of EPNS as functions of the total baryon density.

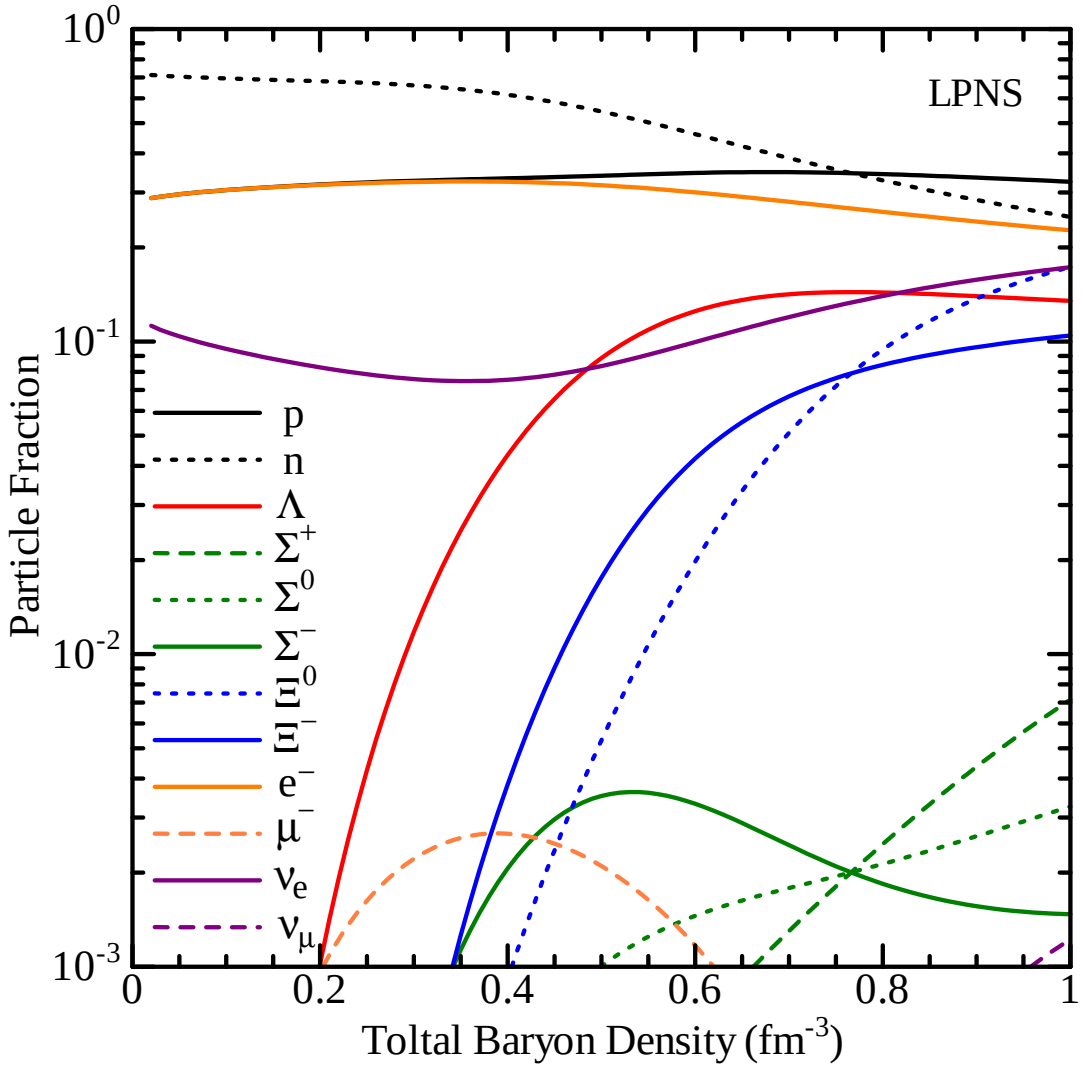

Figure 2: The same as Fig. 1 but for LPNS.

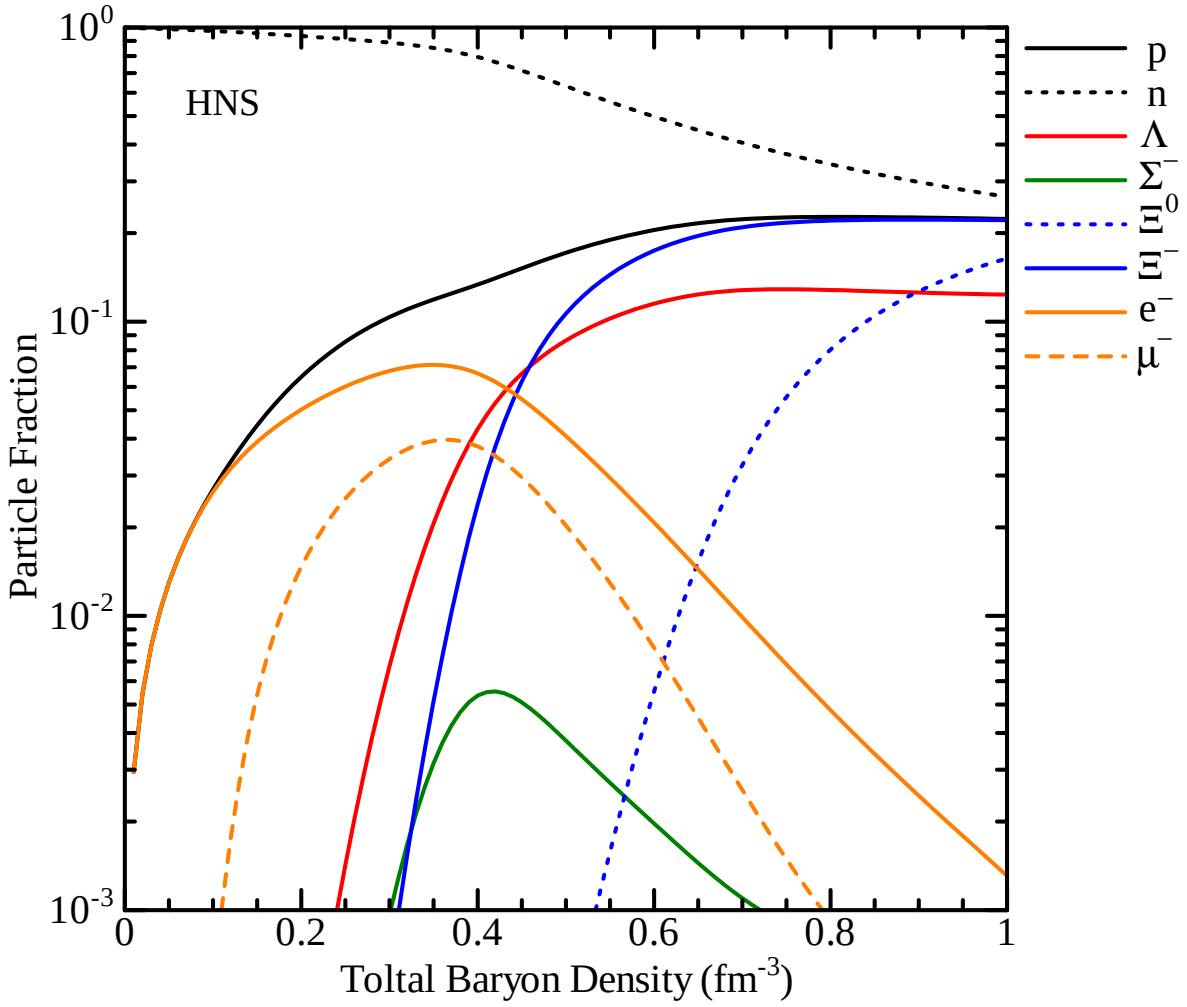

Figure 3: The same as Fig. 1 but for HNS.

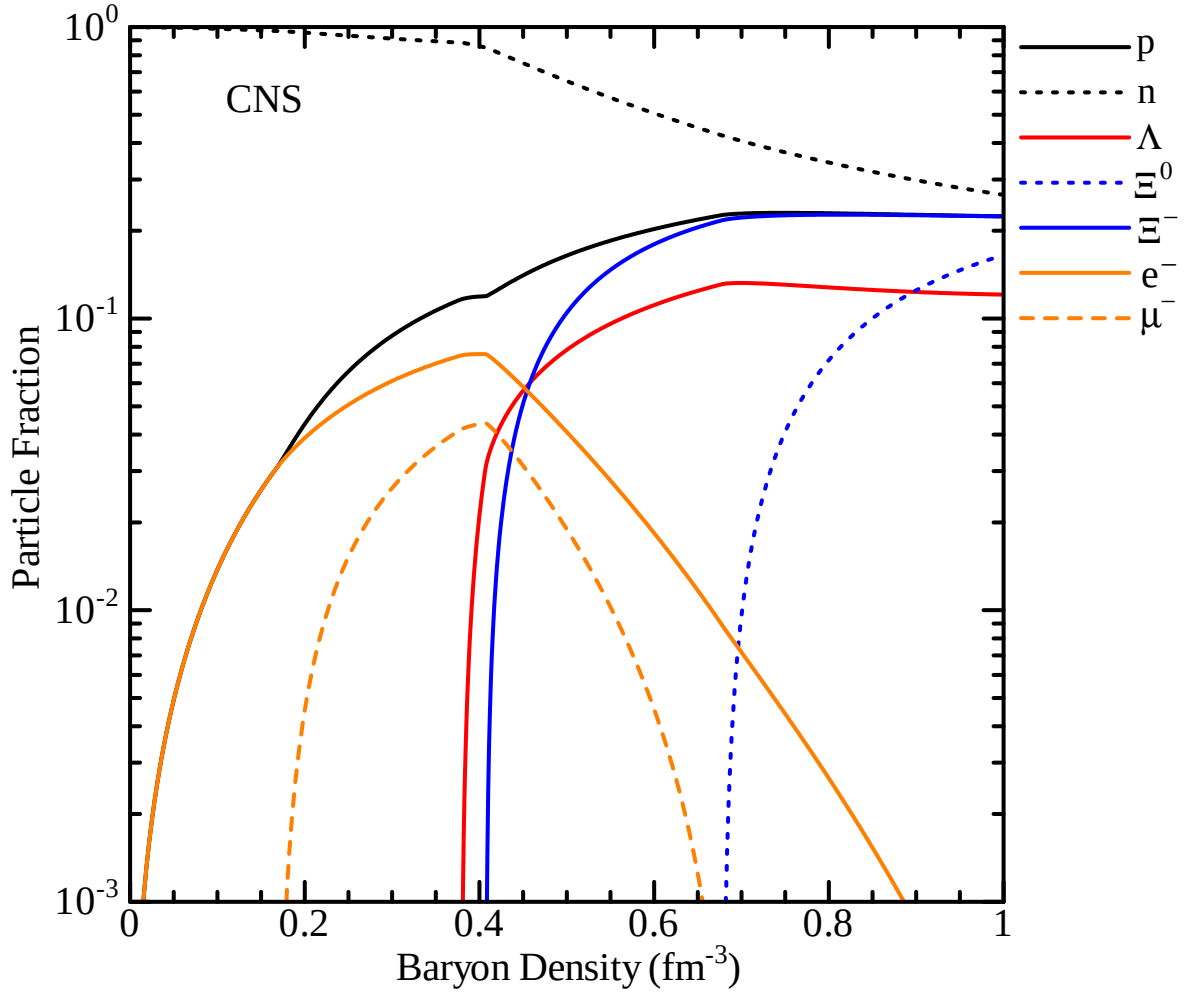

Figure 4: The same as Fig. 1 but for CNS.

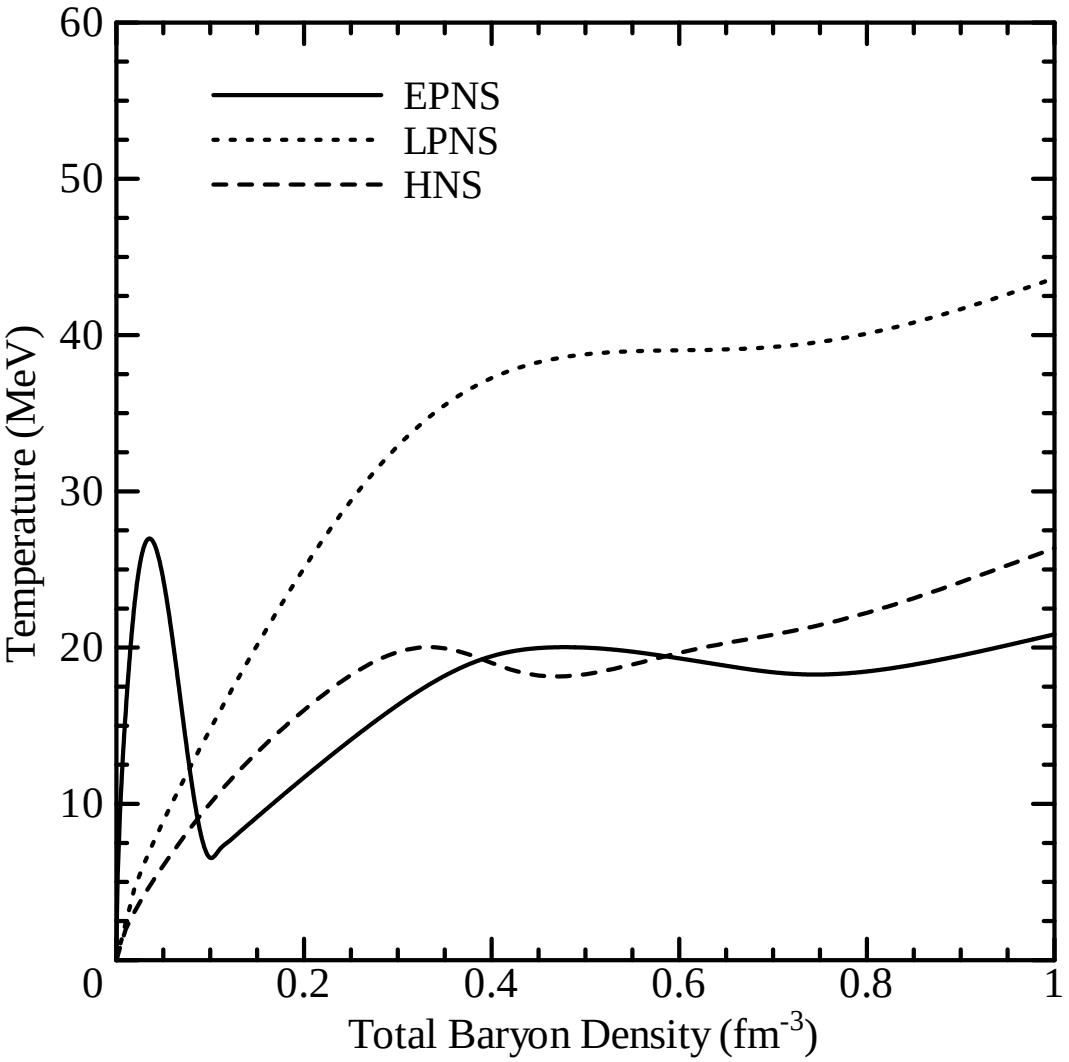

Figure 5: The temperature profiles in EPNS, LPNS and HNS.

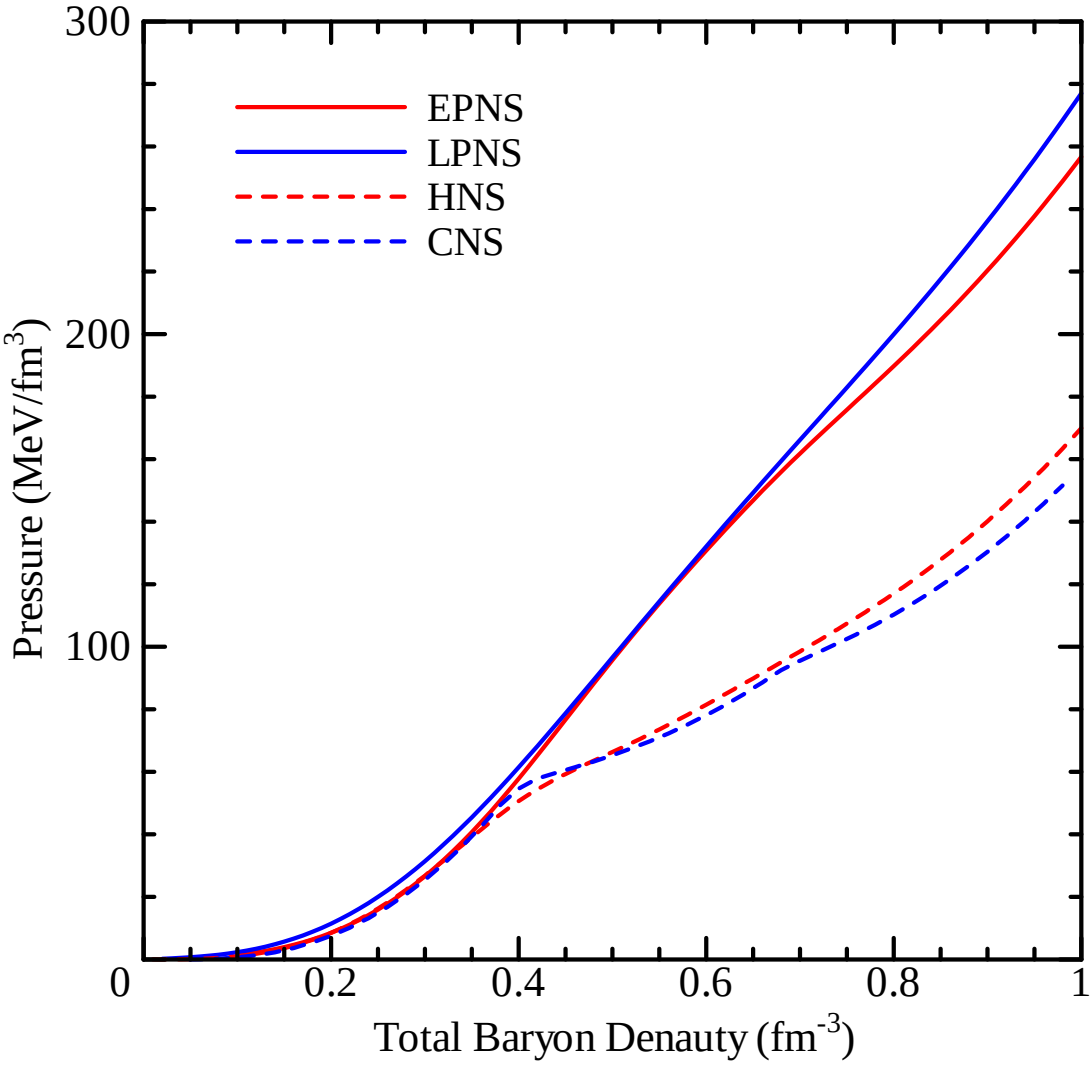

Figure 6: The pressures in EPNS, LPNS, HNS and CNS as functions of the total baryon density.

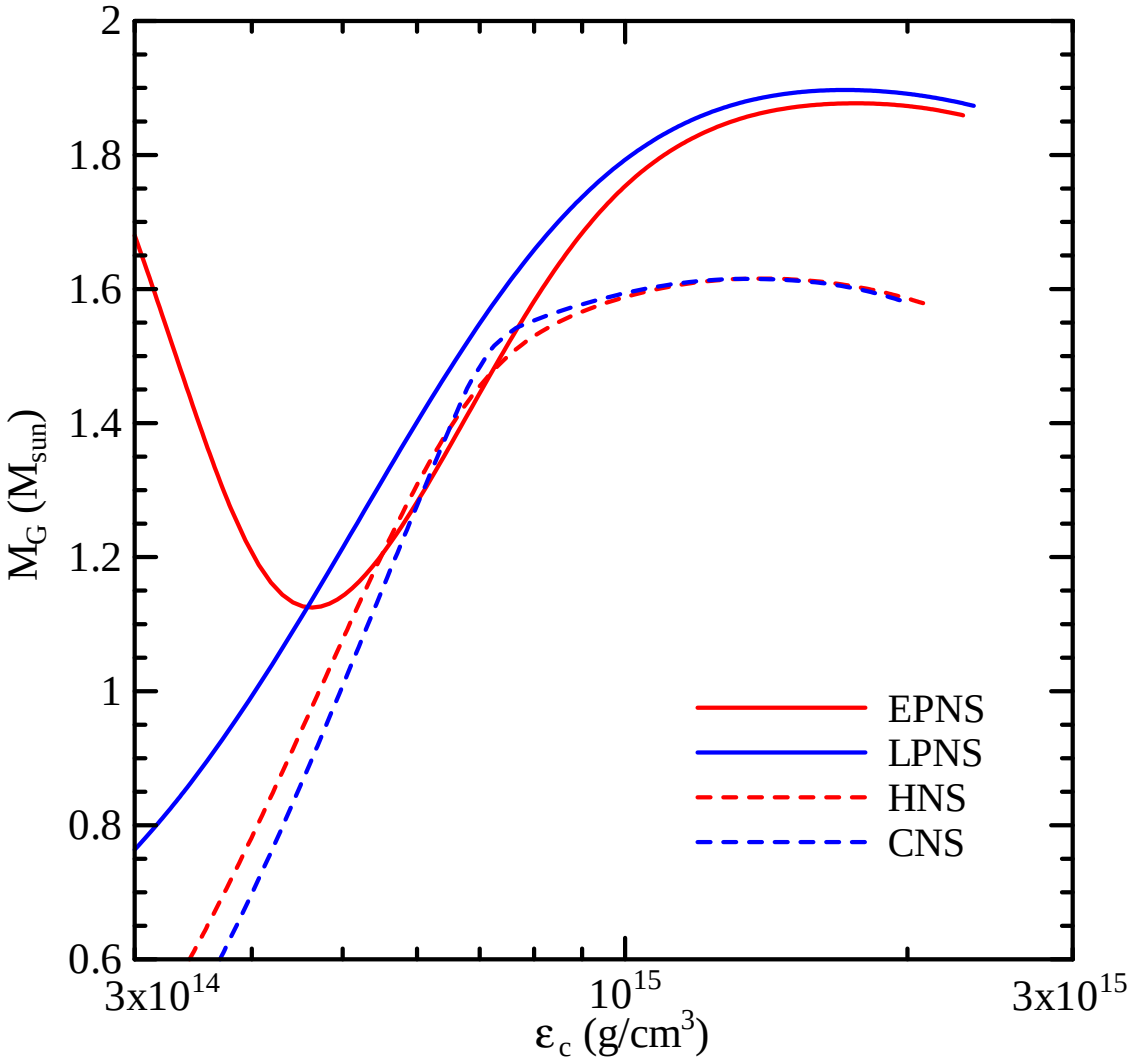

Figure 7: The gravitational masses of EPNS, LPNS, HNS and CNS as functions of the central energy density.

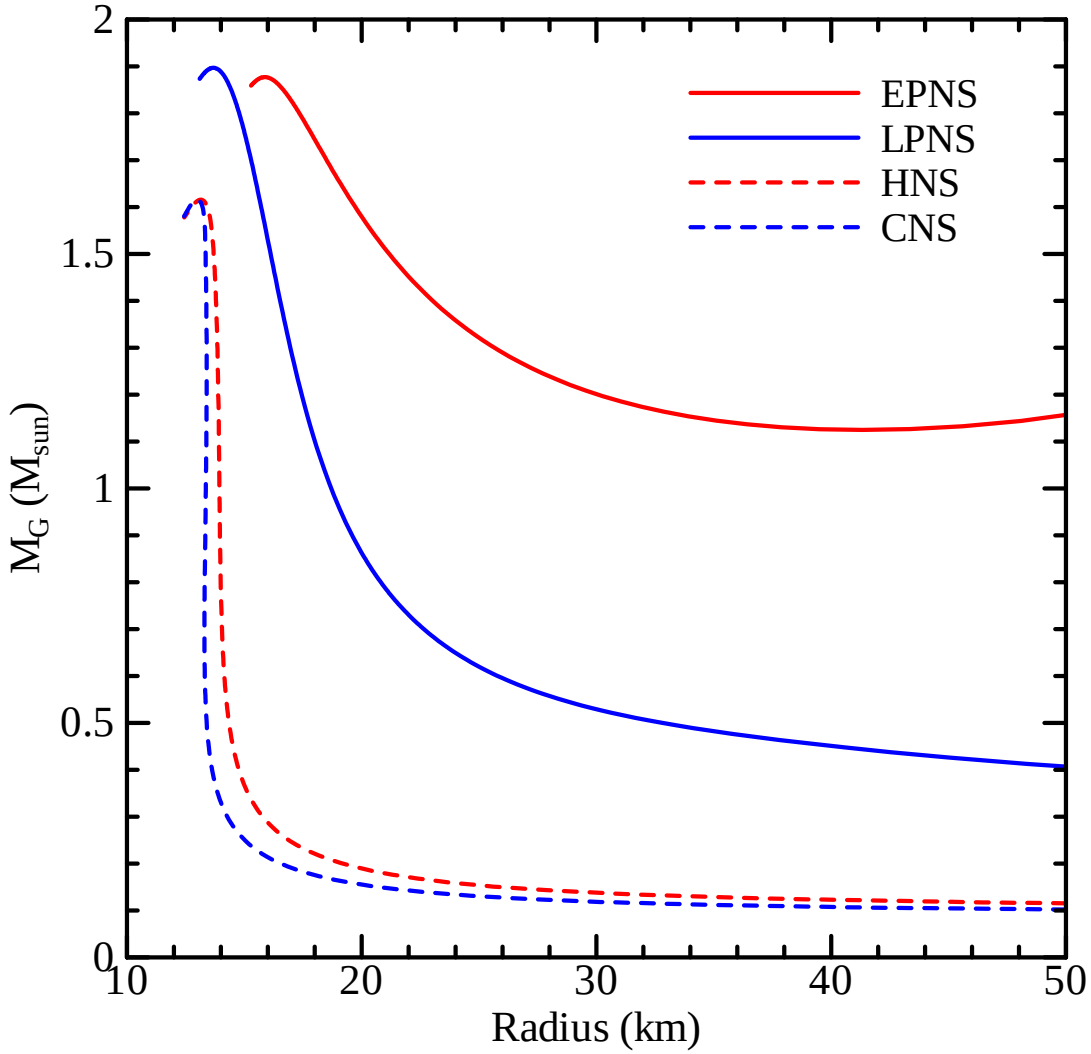

Figure 8: The gravitational masses of EPNS, LPNS, HNS and CNS as functions of the radius.

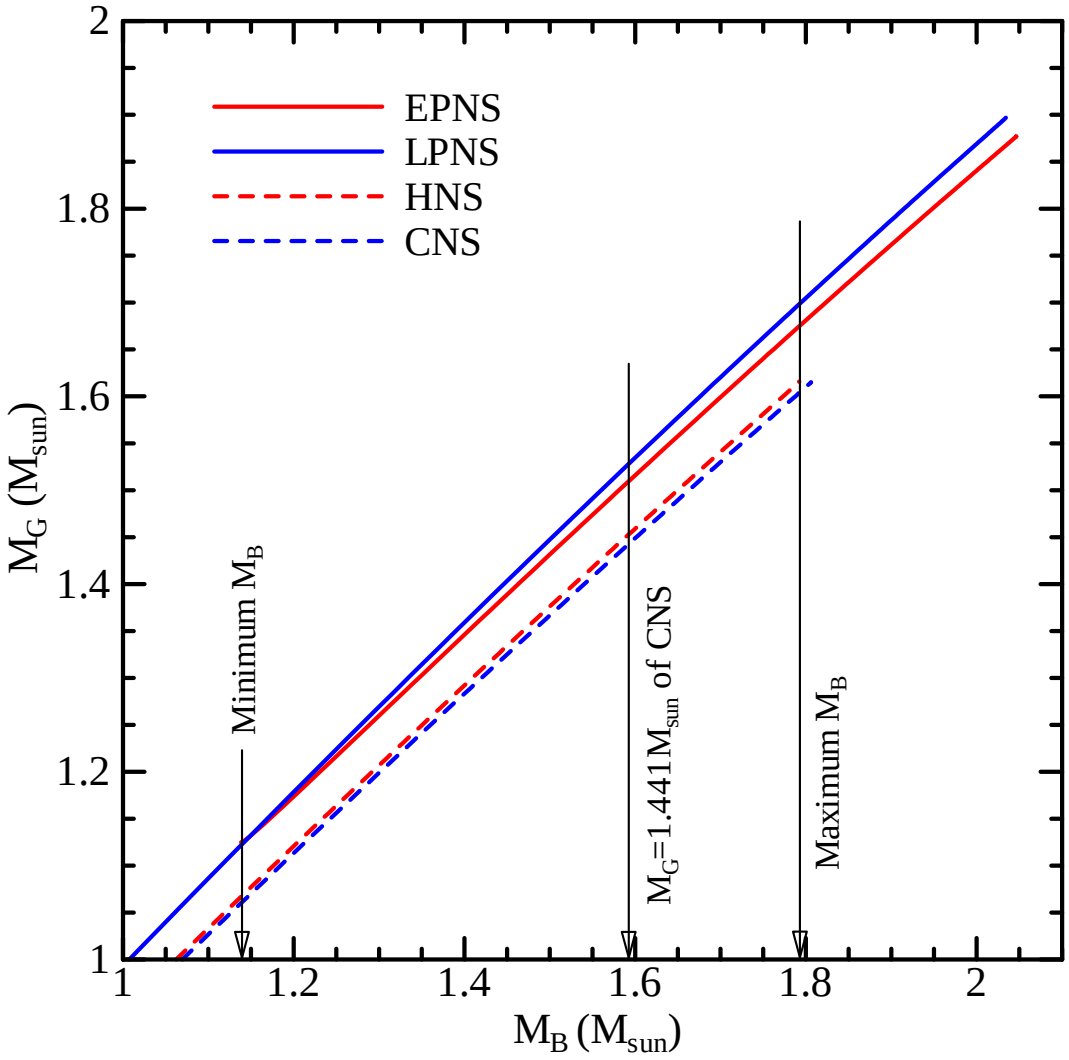

Figure 9: The gravitational masses of EPNS, LPNS, HNS and CNS as functions of the baryonic mass.

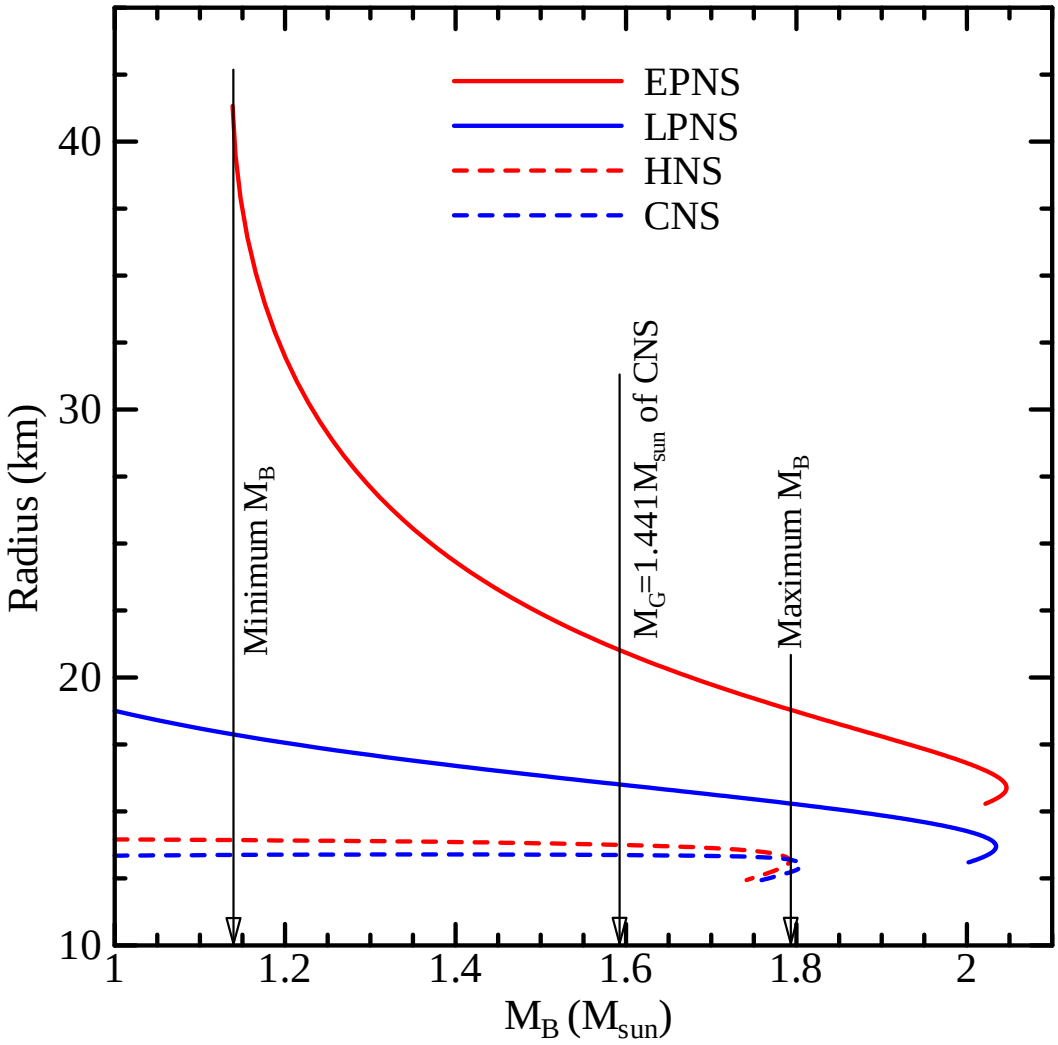

Figure 10: The same as Fig. 9 but for the radius.

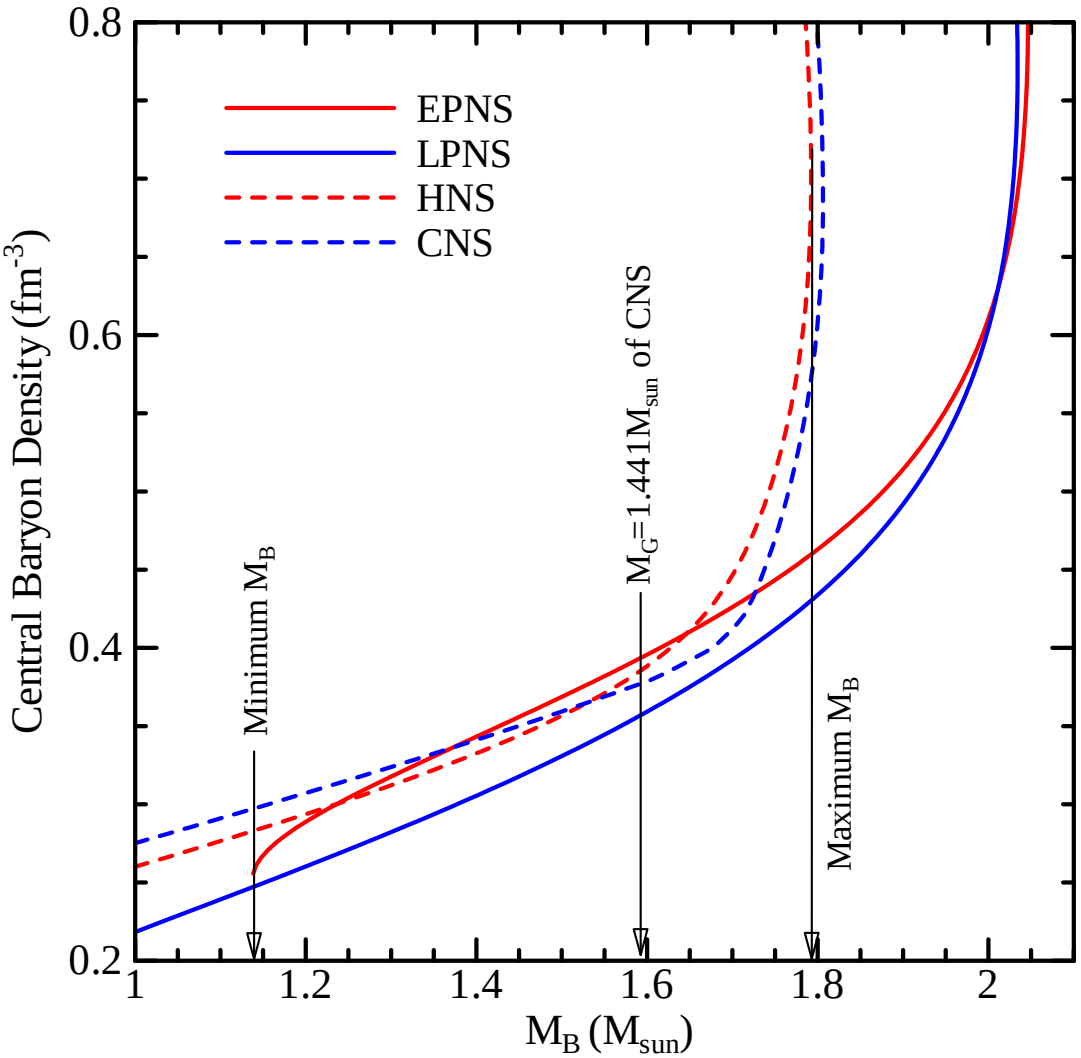

Figure 11: The same as Fig. 9 but for the central baryon density.